

STATIC AND FATIGUE TESTING OF FULL-SCALE FUSELAGE PANELS
FABRICATED USING A THERM-X^{®*} PROCESS

P. 26

Albert J. DiNicola, Christos Kassapoglou, and Jack C. Chou^{**}
UNITED TECHNOLOGIES-Sikorsky Aircraft Division
Stratford, CT

SUMMARY

Large curved integrally stiffened composite panels representative of aircraft fuselage structure were fabricated using a Therm-X[®] process, an alternative concept to conventional two-sided hard tooling and contour vacuum bagging. Panels subsequently were tested under pure shear loading in both static and fatigue regimes to assess the adequacy of the manufacturing process, the effectiveness of damage tolerant design features cocured with the structure, and the accuracy of finite element and closed-form predictions of postbuckling capability and failure load. Test results indicated the process yielded panels of high quality and increased damage tolerance through suppression of common failure modes such as skin-stiffener separation and frame-stiffener corner failure. Finite element analyses generally produced good predictions of postbuckled shape, and a global-local modelling technique yielded failure load predictions that were within 7% of the experimental mean.

INTRODUCTION

The manufacture of large composite airframe fuselage structure is greatly facilitated whenever preimpregnated skin, longeron, and frame layups are cocured. A degree of inherent damage tolerance also may be built into the cocured structure by using design concepts which, by their very nature, suppress fundamental postbuckled composite panel failure modes. Conventional manufacturing requirements for cocuring curved stiffened panels mandate the use of precise two-sided hard tooling along with intricate contoured vacuum bagging to ensure high quality consolidation while minimizing defects such as ply wrinkling, fiber bridging, or internal voids. Simplification of both tooling and vacuum bagging requirements would further enhance the cost effectiveness of cocuring.

A manufacturing process using the silicon-based powder polymer Therm-X[®] as a pressure transfer medium was shown to reduce hard tooling and simplify vacuum bagging procedures for cocured skin-hat

Work performed under NASA Contract NAS1-18799 through the Langley Research Center, Contract Monitor Jerry W. Deaton.

* Therm-X is a product of the DOW Co.

** Currently with UNITED TECHNOLOGIES-Pratt and Whitney GEB

stiffener and skin-inverted T stiffener building block test specimens [1]. The capability of the same Therm-X process to produce large cocured integrally stiffened fuselage panels with comparable integrity to that noted in [1] was evaluated during this investigation. Specifically, panels were tested under pure shear loading in both static and fatigue environments.

The postbuckled behavior of stiffened composite panels has been investigated by a number of other authors. Prediction of the initial buckling load of stiffened panels, which is often several times less than the ultimate failure load, is usually done through closed-form analyses with various uniform boundary conditions and assumed mode shapes. Due to the complexity of the postbuckled problem formulation, e.g., geometric nonlinearities with intermediate boundary conditions (neither simply supported nor fully clamped), finite element investigations commonly are used instead. References [2-4], for example, used geometrically nonlinear finite element formulations to study the problem of stiffened composite panels loaded in compression. The results cited by these authors indicate generally good correlation between predicted and observed load-deflection behavior but not as good correlation of internal loads, moments, and strains throughout the postbuckled state. Lack of correlation was attributed to initial manufacturing imperfections which were not considered in the numerical studies. The postbuckled behavior of a simply curved multibay stiffened aluminum panel loaded in pure shear was investigated by Jarlas [5]. The physical dimensions of each bay were similar to the composite bays considered in this study. Although the initial buckling load was accurately predicted, convergence difficulties precluded an assessment of overall panel strength while postbuckled. A comprehensive test and analysis program aimed at quantifying postbuckled behavior of curved integrally stiffened panels under combined shear and compression loads was carried out by Ogonowski and Sanger [6]. Approximate closed-form predictions of initial buckling loads and postbuckled load distribution were done using a characteristic panel bay under combined loading. Edge support conditions were either simply supported or clamped on all four sides. In general, all closed-form predictions of postbuckled strength served as upper bounds on experimental results. However, an assessment of local stress states which would initiate failure was not available in closed-form.

In this investigation, prediction of the static failure load of the postbuckled composite panels was done using both closed form methods and finite element analyses. The closed-form method used a modification of the classic diagonal tension analysis developed by Kuhn [7] which accounted for the orthotropic nature of the composite panel [8]. Geometrically nonlinear finite element analyses were used to provide additional information regarding the local states of stress at failure. Using output of a global finite element model, refined local finite element models were built of the vicinity of observed failure locations to investigate local stress states throughout the postbuckled panel.

An investigation of the behavior of one postbuckled panel under cyclic loads was performed. Constant amplitude loading was applied

where the load intensity produced prebuckled and postbuckled skins for the minimum and maximum loads, respectively. The significance of damage growth monitored during the test is discussed.

AUTOCLAVE THERM-X® PROCESS

Two-sided hard tooling, the conventional concept for cocuring, serves the dual function of properly positioning prepreg layups and evenly distributing autoclave pressure to the composite during the cure cycle. Vacuum bags must conform closely to the surfaces where hard tooling cannot contact the prepreg in order to properly transmit autoclave pressure. Errors in tool positioning can produce undesirable results such as stiffener misalignment, skew, and twist. Inadequate vacuum bag contouring can produce fiber bridging and poor compaction of radius features. Relaxation of tooling and bagging requirements would greatly promote the use of cocure strategy as a viable and economical means of composite manufacture.

A cocure manufacturing concept which takes advantage of the flow characteristics of the silicon-based polymer Therm-X and thereby reduces tooling and bagging requirements has been demonstrated by the authors [1]. Under ambient pressure the Therm-X medium is in the form of a fine powder. When subjected to autoclave pressure, however, the powder exhibits flow characteristics similar to liquid media. In this pressurized flowable state the polymer transmits quasi-hydrostatic pressure to the prepreg that is equal to the applied autoclave pressure. Upon venting to atmospheric pressure, Therm-X reverts back to its powdery state thereby permitting easy tool breakout and laminate removal. There appears to be no limit to the number of times a quantity of Therm-X may be reused in the manner described above.

The advantages of the autoclave cocuring process which uses Therm-X are two-fold. First, only one-sided hard tooling is needed to position the prepreg since hydrostatic pressure exerted by the medium ensures even pressure distribution. Second, only the Therm-X containment vessel (discussed below), and not the entire contour of the laminate, must be vacuum bagged because the magnitude of the pressure within the contained volume of Therm-X depends only on the magnitude of externally applied autoclave pressure.

Fabrication of the curved integrally stiffened panels used in this study was done as outlined in the series of illustrations shown in Figure 1. Note the use of one-sided hard tooling for the frame (inverted T) stiffeners as well as the simplicity of the final vacuum bagging procedure.

STIFFENED PANEL DESIGN

In order to generate test and analysis information that would be most useful to the industry in general, the test articles were designed to be representative of fixed wing fuselage or rotary wing tailcone structure; see Figure 2. The panel measured 30 inches per edge with

a radius of curvature equal to 40 inches. The skin in the panel bays was made of woven graphite/epoxy (Gr/Ep) oriented 45 degrees to the hat stiffeners and measured 0.030" thick. The frame layup was a symmetric combination of woven and tape forms of Gr/Ep which measured 0.078" thick. Hat stiffener webs were 0.015" thick and made of woven Gr/Ep. Hat stiffener caps were made from a combination of woven and tape Gr/Ep and ranged from 27 to 35 mils thick. In an undamaged condition, the panel was designed to carry an ultimate load of 250 lb/in shear flow per edge. A damage tolerance static strength knockdown of 50% was assumed. To satisfy the damage tolerance ultimate load criterion, the panel should exceed 500 lb/in shear flow at failure.

The objectives of the damage tolerance design features incorporated into the panel were to suppress skin-stiffener separation, a common failure mode of postbuckled panels, and maintain frame-longeron load transfer in the postbuckled state. Stiffener-skin separation which precipitated overall loss of panel stiffness was the most common failure mode observed in Reference [6]. The interface between the skin and stiffener was most often the weakest link in the postbuckled structure because the longerons and frames were cocured directly on top of the skin thereby promoting a free edge induced interlaminar tension stress field. The stiffener-skin separation problem has been investigated by various authors [9,10]. A design alternative which suppresses the separation failure mode is shown in Figure 3 and will henceforth be referred to as the embedded flange design concept. Covering stiffener flange free edges with one ply of skin was expected to reduce the propensity for separation by effectively suppressing the interlaminar tension stress field. Additionally, cocured shear ties between frames and longerons were used in the specimen design, see also Figure 3. These load transfer mechanisms were believed to increase the structural integrity of the panel by ensuring load path continuity in the postbuckled state.

TEST DESIGN

A "picture frame" fixture was used to introduce pure shear loading into the specimens. The fixture consisted of four equal length steel I-beam sections pinned at each end to form a square frame enclosing the test article; see Figure 4. Aluminum brackets fastened to the webs of each I-beam were used to restrain the specimens during test. Application of loads along the diagonal as shown in Figure 4 produced nearly pure edgewise shear on the specimen. Loads were applied using an MTS 810 testing machine. Detailed finite element models, with the specimen and fixture modelled explicitly, confirmed that very nearly pure shear was introduced to the panel's two central bays. The fatigue investigation was conducted using the same fixture and MTS unit. Constant amplitude fatigue loads equal to two-thirds of the damage tolerance ultimate requirement, 330 lb/in edge shear, were applied at a frequency of 0.3 to 0.6 Hz and an R-ratio of 0.1. It was felt this load level would ensure some damage growth during the cyclic test. Damage growth was monitored on a decade schedule throughout the test, i.e. at 1, 10, 100, 1000, etc, cycles. Hand-held ultrasonic pulse-echo equipment as well as close visual

inspections served to monitor the progression of damage. Quasi-static strain gage surveys were also performed on the decade schedule to quantify stiffness loss as a function of cycles.

STATIC TEST: RESULTS AND ANALYSIS

Three specimens were used for static testing. Each specimen was installed in the picture frame shear fixture, Figure 4, and tested under increasing quasi-static load until catastrophic failure was observed. The panel failed by separating into two large sections. Each panel evidenced initial buckling at about 96 lb/in applied load. The experimental average failure load was 580 lb/in edge shear which corresponds to a postbuckling ratio (PBR) of 6. Each individual test result was in excess of the 500 lb/in damage tolerance ultimate requirement. A summary of initial buckling loads, catastrophic failure loads, and the postbuckling ratio for all specimens is provided in Table 1.

Prior to reaching the initial buckling load, the deflection at the center of the panel was in the direction of the normal to the outer surface (convex side) of the panel. Once the applied load exceeded the initial buckling load a reversal in center panel deflection was observed. From this point onward center deflections were directed along the normal to the inner surface of the panel. While in a postbuckled configuration each panel bay exhibited the classical diagonal buckled pattern, shown in Figure 5 for a load level of 283 lb/in.

Close monitoring of damage generation and growth during testing of panel #3 was representative of all panels. At 487 lb/in shear flow (PBR=5), a 5 inch crack appeared in the web of one outer hat stiffener and grew to 7 inches as load was increased to 554 lb/in. At that load a 4 inch crack appeared in the skin of one bay along a buckle, emanating from a stiffener intersection and producing a change in buckled pattern. A specimen under 554 lb/in shear flow is shown in Figure 6. Final failure occurred at 611 lb/in applied load and is believed to have been precipitated by the cracks in the hat stiffener webs which propagated through the specimen as shown in Figure 7.

Closed-form prediction of static failure loads for the curved stiffened specimens was done using methodology documented in [8]. For the panels in this study, analytically calculated diagonal tension strains at the average failure load of 580 lb/in were 3200 microstrain at the panel bay's center. Strain gage results from the three static tests at hand were reduced using the membrane strain recommendation [6] wherein back-to-back three-element strain rosettes are used to determine midplane laminate strain. Average membrane strain thus determined was 3450 microstrain, a 7.2% difference from the closed-form prediction.

Although the closed-form analysis yielded good predictions of diagonal tension strain at failure, the method is incapable of providing information regarding failure initiation in the hat

stiffener webs. A detailed stress analysis is required to obtain information sufficient to perform a local strength evaluation. A finite element model of the specimen and fixture shown in Figure 8 was run using the geometrically nonlinear solution sequence SOL 66 in MSC/NASTRAN. The iterative solution scheme was controlled through an applied displacement increment technique. At the average failure load of 580 lb/in, the analysis was stopped and all nodal displacements and rotations were output. These finite element results will be referred to as the global solution in the discussions which follow.

As noted above, failure of the specimens was believed to have originated in the webs of the hat stiffeners. Observed local buckles in these webs were thought to have precipitated catastrophic failure. In the global finite element model of the entire specimen the total height of the web was modelled with only one element; see Figure 9. The admissible displacement field of the web, linear between nodes, could not capture the local buckles experimentally observed and as a result could not yield accurate local stress values. For this reason, local modelling efforts focused on the most highly loaded webs, denoted 1 and 3 in Figure 9.

The local finite element model of the entirety of the web of hat stiffener 1 is shown in Figure 10. The height of the web in the local model was modelled using six elements which should allow local buckles to be analytically captured. Boundary conditions around the perimeter of the model were applied by means of specified nodal displacements and rotations at nodes of the local model with exact correspondence to nodes of the global model. These corresponding nodes are circled in the figure. Linear interpolation of all boundary conditions was used for local model boundary nodes in between the nodes with correspondence. The total displacements and rotations from the global model which were associated with the average failure load of 580 lb/in were applied to the boundary of the local model in forty equal increments. The geometrically nonlinear solution scheme used for the global model was used for the local analysis.

At the boundary conditions associated with 580 lb/in edge load, the deflected shape obtained using the local model is shown in Figure 11. The twisting undulations of the web from the leftmost to the rightmost edge shown in this figure were noted during static tests.

The Hoffman criterion [11] was used to assess failure in each finite element. The form of the criterion is defined through the Hoffman Failure Number (HFN):

$$HFN = 1 - (S_{11}^2/X_t X_c) - (S_{22}^2/Y_t Y_c) - (S_{11} S_{22}/X_t X_c) - (X_c - X_t) S_{11}/X_t X_c - (Y_c - Y_t) S_{22}/Y_t Y_c - (S_{12}^2/T^2) \quad (1)$$

when $HFN > 0$, no failure of ply,
 when $HFN \leq 0$, failure of ply,

where S_{11} = calculated stress in fiber (or warp) direction,
 S_{22} = calculated stress in transverse (or fill) direction,
 S_{12} = calculated in-plane shear stress,
 X_t, X_c = tension, compression strength in fiber direction,
 Y_t, Y_c = tension, compression strength transverse direction,
 T_t, T_c = in-plane shear strength

The criterion allows unequal values of tension and compression strength in the material directions.

Classical laminated plate theory was used to calculate material coordinate system stresses for Eq. (1). Transverse shear loads calculated in the local model were noted to be small and judged not to contribute to failure. Hoffman Failure Numbers for mean strength allowables are presented graphically in Figure 12. The lowest margin lies between contour E and 0.0, the exact value being 0.072. Assuming stresses to scale linearly with load, an acceptable approximation at this point of the postbuckled analysis, the percent error between the analysis and average test results is 7.2%.

A photograph of the location corresponding to the smallest margins in Figure 12 is shown in Figure 13. The photograph was taken from panel #3 after failure. The prediction in Figure 12 is for failure at the top of the web while the observed crack was nearer the bottom. This discrepancy is probably due to either slight boundary overconstraint along the top edge of the model which acts as a modest "load sink" or locally reduced material strength.

The two damage tolerance design features, embedded stiffener flanges and cocured shear ties, performed effectively in the postbuckled regime. As expected, stiffener-skin separation failure modes were suppressed by the embedded flange design. Cocured shear ties remained intact even upon catastrophic failure and as a result were judged to be an effective means of maintaining load transfer between intersecting stiffeners.

FATIGUE TEST: RESULTS AND ANALYSIS

One constant amplitude cyclic load fatigue test was performed. It was decided the specimen should produce some damage growth in order to investigate the fatigue capacity of the panel. The maximum fatigue load was selected to be two-thirds of the damage tolerance static ultimate requirement, 330 lb/in edge shear (PBR=3.5). Loss of panel stiffness was monitored through the six strain gage rosettes shown in Figure 14. Substantial life at this maximum load level would demonstrate damage tolerance of the panel under the fatigue environment.

An illustration of the buckled shape of the panel during the first loading cycle is shown in Figure 15. Note the hat stiffeners acted as buckled waveform breakers across which buckling patterns were not continuous. Initial buckling of the panel occurred in the neighborhood of 96 lb/in edge shear, similar to the static tests.

The extension of several visible cracks, denoted A, B, C, and D, during the first 10,000 cycles is highlighted in Figure 16. Based on experience gained during static testing these cracks mainly provided relief of local stress concentrations due to the picture-frame shear loading configuration and did not influence the fatigue life of the panel. The fact that progress of these cracks was arrested for a long time prior to final failure lent validity to the argument. Inspections of the entire panel according to the decade schedule yielded no indications of nonvisible damage.

The test was continued until further damage was noted, see locations E and F in Figure 16. The extent of these delaminations was quantified using a pulse echo ultrasonic technique at the cyclic intervals shown. Once again, these delaminations were judged to relieve local stress concentrations due to the loading configuration and, therefore did not adversely affect the total life of the part. No visible or nonvisible damage in addition to that shown in Figure 16 was identified.

The first significant failure occurred at 69,200 cycles. This failure initiated in both webs of one of the outer hat stiffeners as shown in Figure 17. The cracks were easily visible with the unaided eye and were located approximately halfway between the root and top of the web along the stiffener axis. Extension of the cracks to the sizes shown occurred in a single cycle. Ultrasonic inspection found no new nonvisible damage. The buckled shape of the panel after the first significant failure is presented in Figure 18. Note that while the two undamaged hat stiffeners continued to function as panel breakers, the failed stiffener did not.

Immediately following failure of the hat stiffener, the panel was statically tested to a load of 385 lb/in edge shear, two-thirds of the average ultimate load of 580 lb/in. This test established limit load capability of the damaged panel and served to certify the panel up to that load level and equivalent service flight hours. A second hat stiffener failed at 387 lb/in edge shear, 100% of the test requirement. The failure initiated in the webs of the central hat stiffener at the frame-stiffener intersection corner and grew unstably to the dimensions shown in Figure 19. Nonvisible delamination areas also shown in Figure 19 at the flanges of the two damaged stiffeners were found using pulse echo techniques. All previously existing cracks, which were theorized to be stress relief cracks only and not life limiting cracks, did not extend during this test.

The buckled shape of the panel after the second stiffener failure is shown in Figure 20. Note the central hat stiffener is no longer completely effective as a waveform breaker but the intact stiffener remains effective.

Further cycling of the panel to 200,000 cycles was started immediately following the latter static test. Additional nonvisible damage resulting from this cycling is shown in Figure 21. No new visible cracks initiated during this interval.

As shown in Figure 22, rosettes 3-6 demonstrated significant increases of up to 80% measured shear strain after the test to 385 lb/in. The jumps in strain were interpreted to represent a significant redistribution of load through the specimen which occurred as a result of damage in the two hat stiffeners. At 200,000 cycles the fact that strain readings for rosettes 1 and 2 were 20 to 30% of the values during the first cycle suggests very little load passes through the central bays of the specimen. Rather, the primary load path was around the perimeter of the specimen as evidenced by the sharp increases in strain noted in rosettes 3-6 after the test. Since this new load path no longer worked the gage section of the specimen the fatigue test was discontinued.

A final damage summary for the fatigue test article is provided for convenience in Figure 23.

CONCLUSIONS

Major conclusions resulting from the present investigation are summarized below.

- i) The autoclave Therm-X process used in this investigation can be used to cocure large integrally stiffened curved panels effectively and with a high degree of quality.
- ii) Both closed-form analytical and numerical finite element predictions of static test failure load were good to within 7% of the experimental average. Only the global-local finite element approach could predict the actual location of failure.
- iii) Damage tolerance design ultimate load requirement, 500 lb/in edge shear, was surpassed during all static tests. Average static failure load was 580 lb/in edge shear.
- iv) Constant amplitude fatigue tests with maximum load equal to two-thirds of the damage tolerance ultimate load requirement, i.e. 330 lb/in edge shear, yielded a fatigue life of 69,200 cycles. Residual strength tests demonstrated a second hat stiffener failure at 100% of the target load intensity (two-thirds of the experimental mean).
- v) Damage tolerance design features cocured with the structure, i.e. embedded stiffener flanges and frame-longeron intersection shear ties, were effective by suppressing undesirable failure modes at skin-stiffener interfaces and stiffener intersections during both static and fatigue testing.

ACKNOWLEDGMENT

The authors would like to acknowledge the concerted efforts of the Sikorsky Aircraft Materials and Processes Test Lab staff during all phases of this program. In particular, the contributions of Mr. Dave Tuttle to the success of the test program deserve special mention.

REFERENCES

- [1] Kassapoglou, C., DiNicola, A., and Chou, J., "Structural Evaluation of Composite Fuselage Structure Fabricated Using a Therm-X Process", Proceedings of the 46th Annual Forum of the American Helicopter Society, May, 1990.
- [2] Wiggeraad, J. F. M., "Postbuckling Behavior of Blade Stiffened Carbon-Epoxy Panels Loaded in Compression", NLR MP85019, Amsterdam, February 19, 1985.
- [3] Rohwer, K., "Postbuckling Behavior of Fiber Reinforced Plates and Curved Panels", NASA TT-20094, July 1987.
- [4] Natsiavas, S., et al., "Postbuckling Delamination of a Stiffened Composite Panel Using Finite Element Methods", NASA CR-182803, August 1987.
- [5] Jarlas, R., "Postbuckling Finite Element Analysis of a Stiffened Curved Panel Loaded in Shear", FFA-TN-1988-23, Aeron. Research Inst. of Sweden, May 1988.
- [6] Ogonowski, J., and Sanger, K., "Postbuckling of Curved and Flat Stiffened Composite Panels Under Combined Loads", NADC-81097-60, McDonnell Aircraft Corp., December 1984.
- [7] Kuhn, P., Peterson, J., and Levin, L., "A Summary of Diagonal Tension, Part I - Methods of Analysis", NACA 2661, 1952.
- [8] Deo, R., Agarwal, B., and Madenci, E., "Design Methodology and Life Analysis of Postbuckled Metal and Composite Panels", AFWAL-TR-85-3096, Vol. 1, Northrop Corp., December 1985.
- [9] Kassapoglou, C., and DiNicola, A., "Efficient Stress Solutions at Skin Stiffener Interfaces of Composite Stiffened Panels", AIAA/ASME/ASCE/AHS/ASC 32nd Structures, Structural Dynamics, and Materials Conference, Part 2, Baltimore, MD., 1991.
- [10] Hyer, M., and Cohen, D., "Calculation of Stresses and Forces Between the Skin and Stiffener in Composite Panels", AIAA Paper 87-0731, 28th SDM Conference, Monterey, CA., 1987.
- [11] The Behavior of Structures Composed of Composite Materials, Vinson, J., and Sierakowski, R., Martinus Nijhoff Publishers, Dordrecht, the Netherlands, 1987.

TABLE 1: STATIC TEST RESULTS SUMMARY

SPECIMEN NO	FINAL FAILURE LOAD (LB/IN)	POSTBUCKLING RATIO*
1	566	5.90
2	563	5.86
3	611	6.36
Average	580	6.04

* Based on initial buckling load of 96 lb/in edge shear

List of Figures

Static and Fatigue Testing of Full Scale Fuselage Panels Fabricated Using a Therm-X Process

by

Albert J. DiNicola, Christos Kassapoglou, and Jack C. Chou
UNITED TECHNOLOGIES - Sikorsky Aircraft Division

- Figure 1: Fabrication Sequence for Curved Stiffened Panels
- Figure 2: Representative Fuselage and Tailcone Panels
- Figure 3: Shear-Tie and Embedded Flange Design Concepts
- Figure 4: The Picture Frame Shear Fixture
- Figure 5: Diagonal Buckled Pattern, $q = 283$ lb/in Edge Shear
- Figure 6: Buckled Pattern, $q = 554$ lb/in Edge Shear
- Figure 7: Buckled Pattern, $q = 611$ lb/in Edge Shear
- Figure 8: The Global Finite Element Model
- Figure 9: Hat Stiffener Web Elements - Global Model
- Figure 10: Hat Stiffener Web Elements - Local Model
- Figure 11: Deflected Shape of the Local Hat Stiffener Web Model
- Figure 12: Contours of Hoffman Failure Numbers for the Local Model
- Figure 13: Photograph of Failure Location - Panel #3
- Figure 14: Strain Gage Locations on the Fatigue Test Article
- Figure 15: Buckled Shape During the First Load Cycle
- Figure 16: Stress Relief Cracks and Delaminations
- Figure 17: First Significant Fatigue Failure, $N = 69,200$ Cycles
- Figure 18: Buckled Shape After the First Significant Failure
- Figure 19: Damage At 387 lb/in During Residual Strength Test
- Figure 20: Buckled Shape At 387 lb/in During Residual Strength Test
- Figure 21: Additional Damage, $N = 200,000$ Cycles
- Figure 22: Shear Strain vs. Cycles
- Figure 23: Fatigue Test Damage Summary

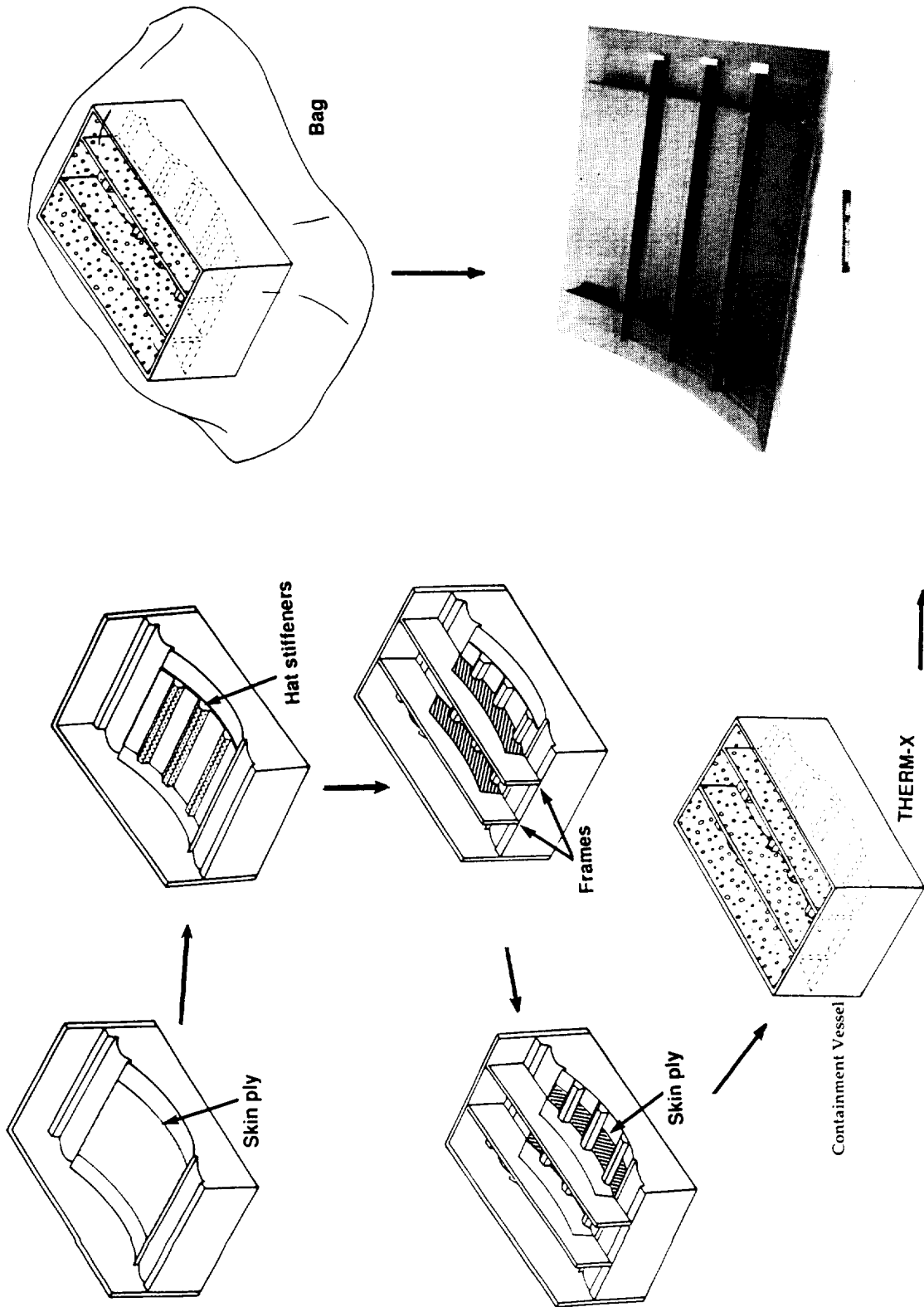


Figure 1A

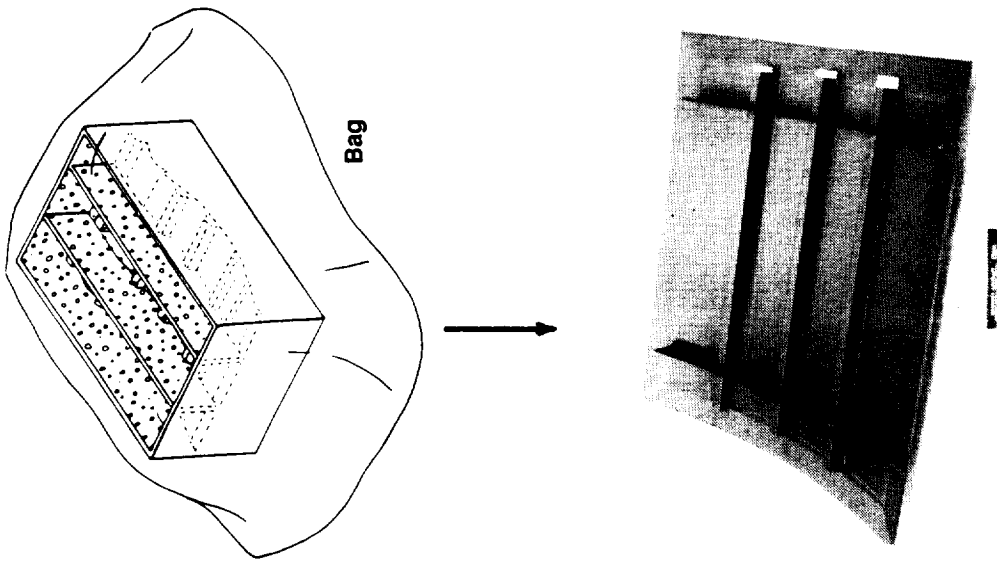


Figure 1B

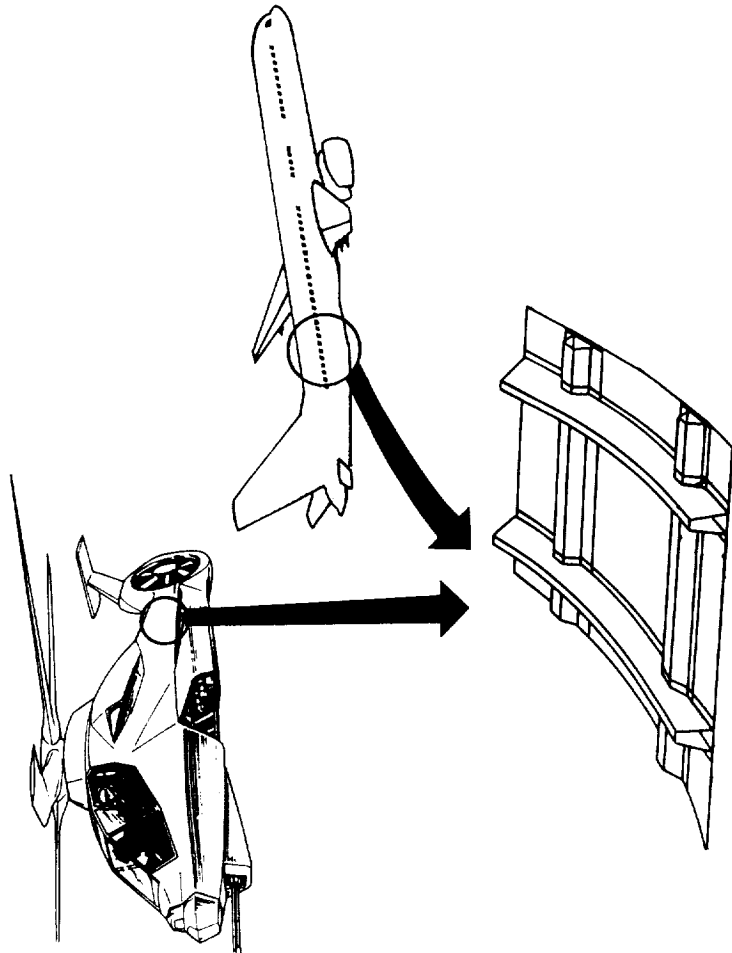


Figure 2

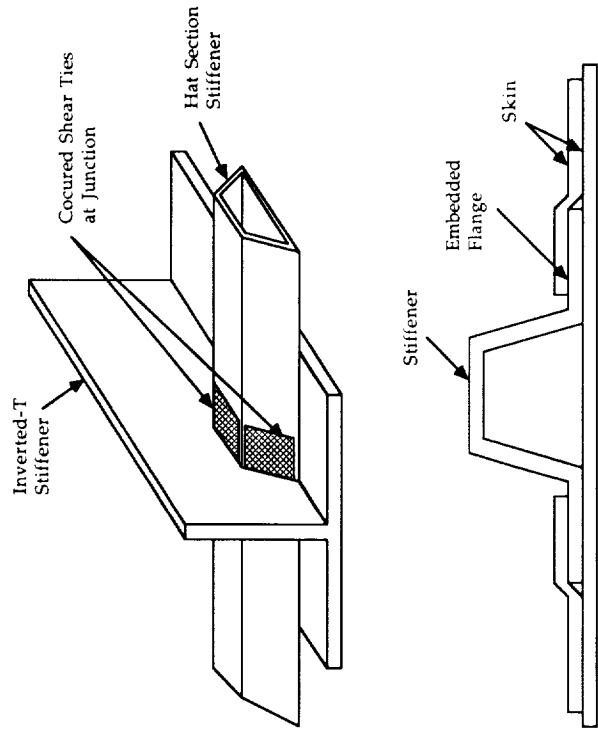


Figure 3

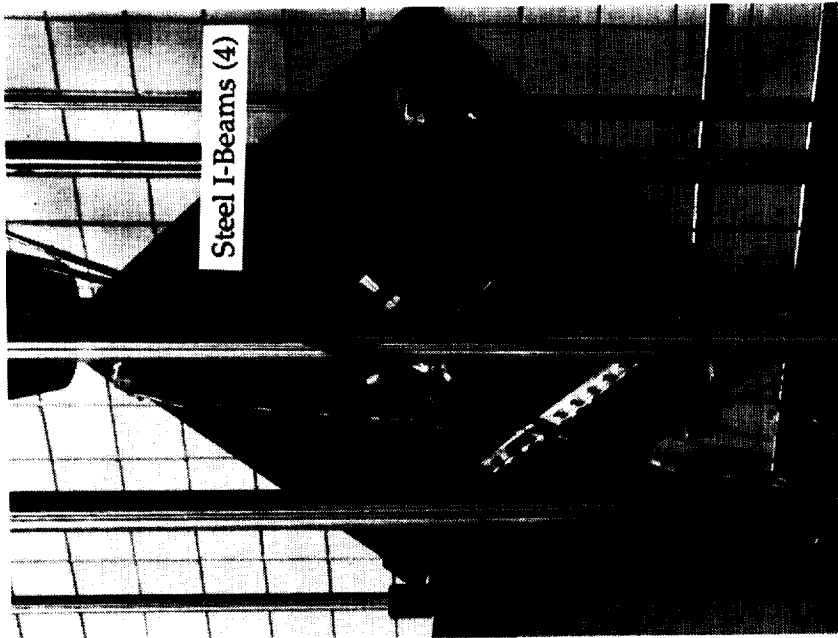


Figure 4

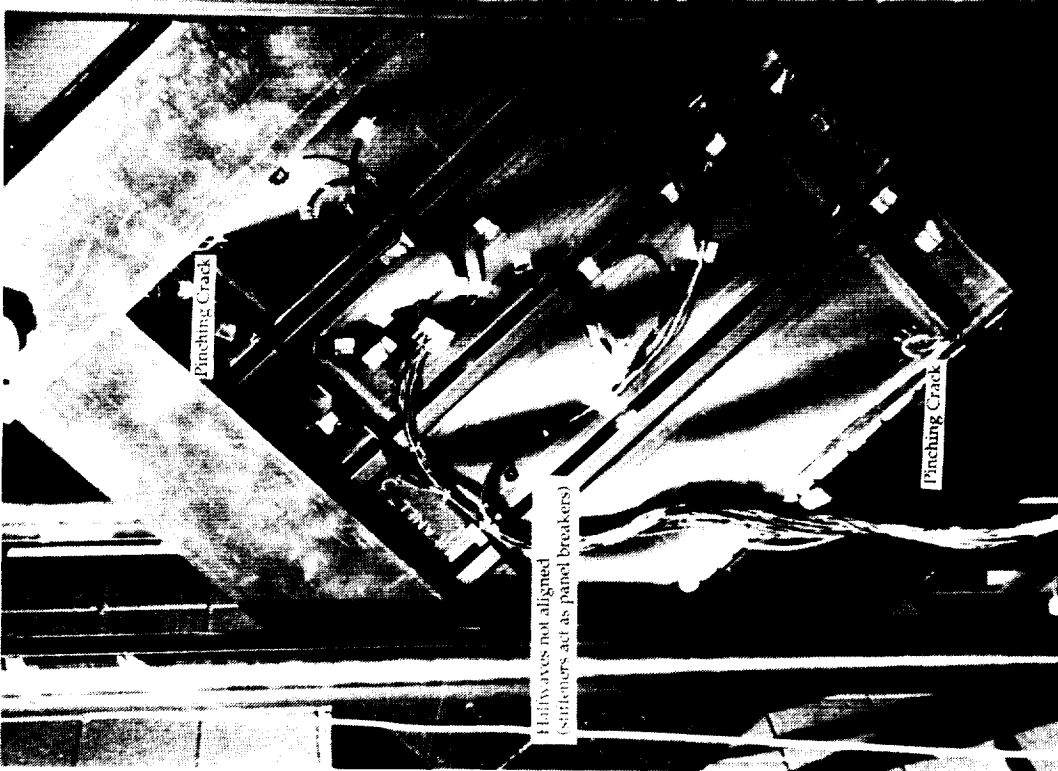


Figure 5

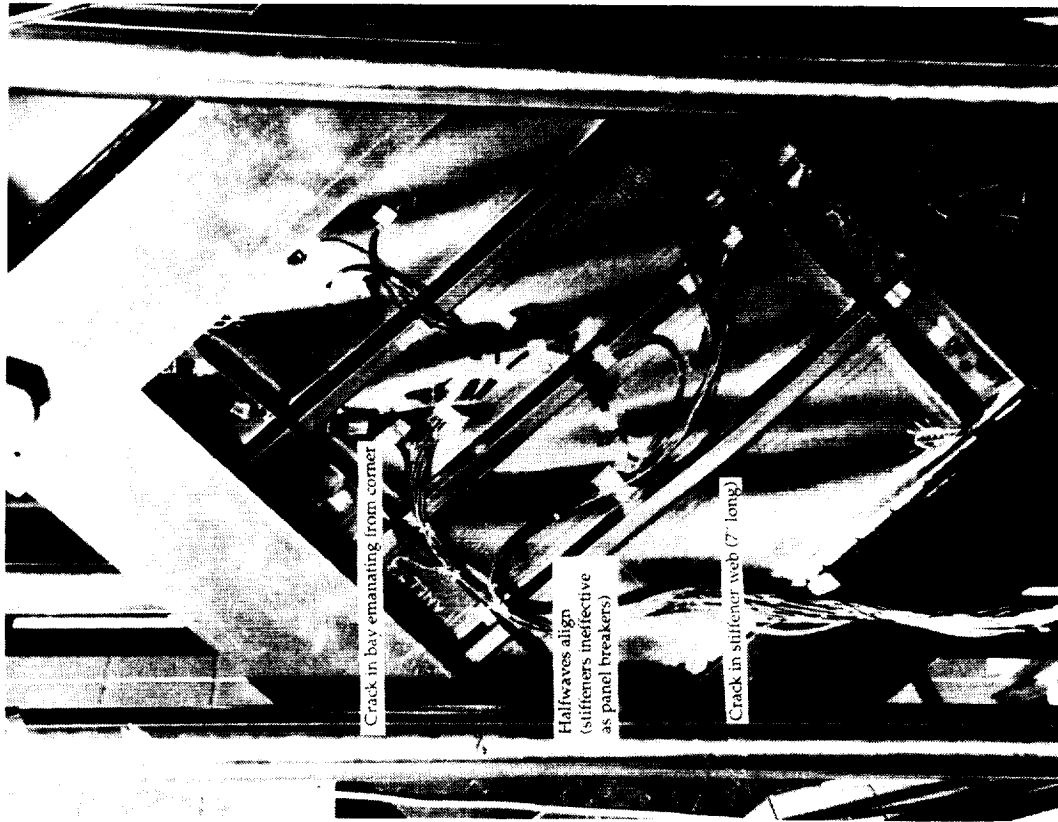


Figure 6

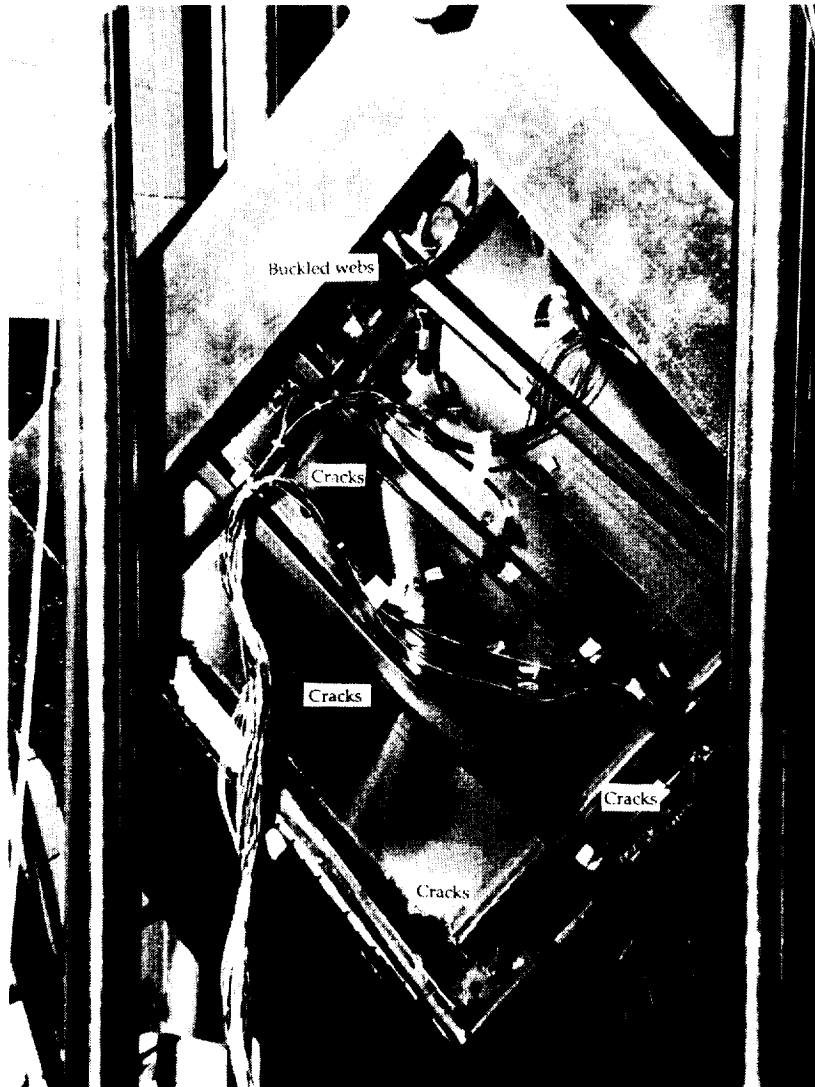


Figure 7

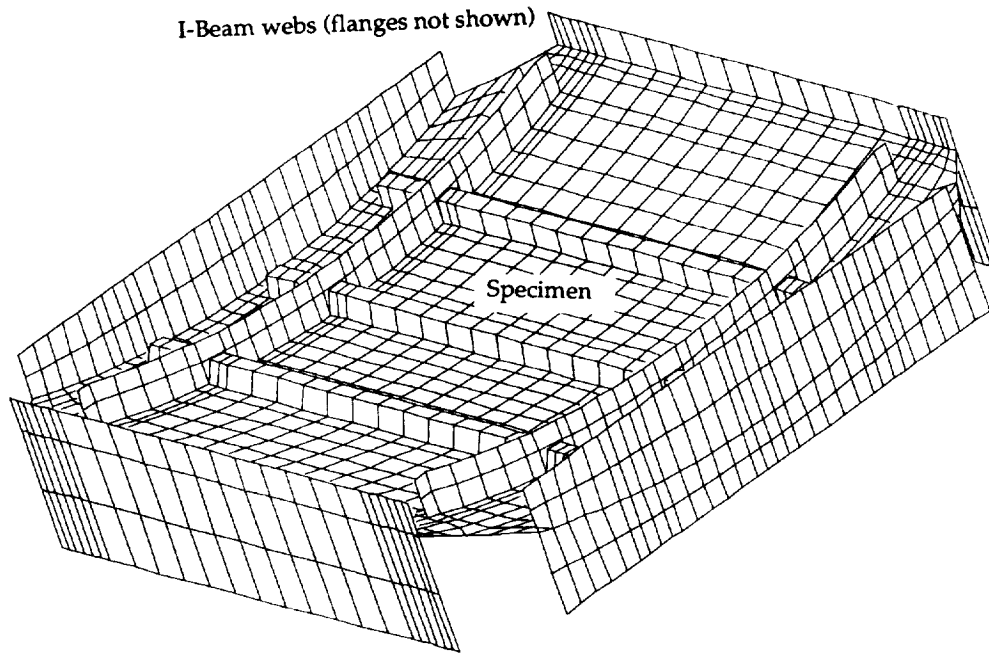


Figure 8

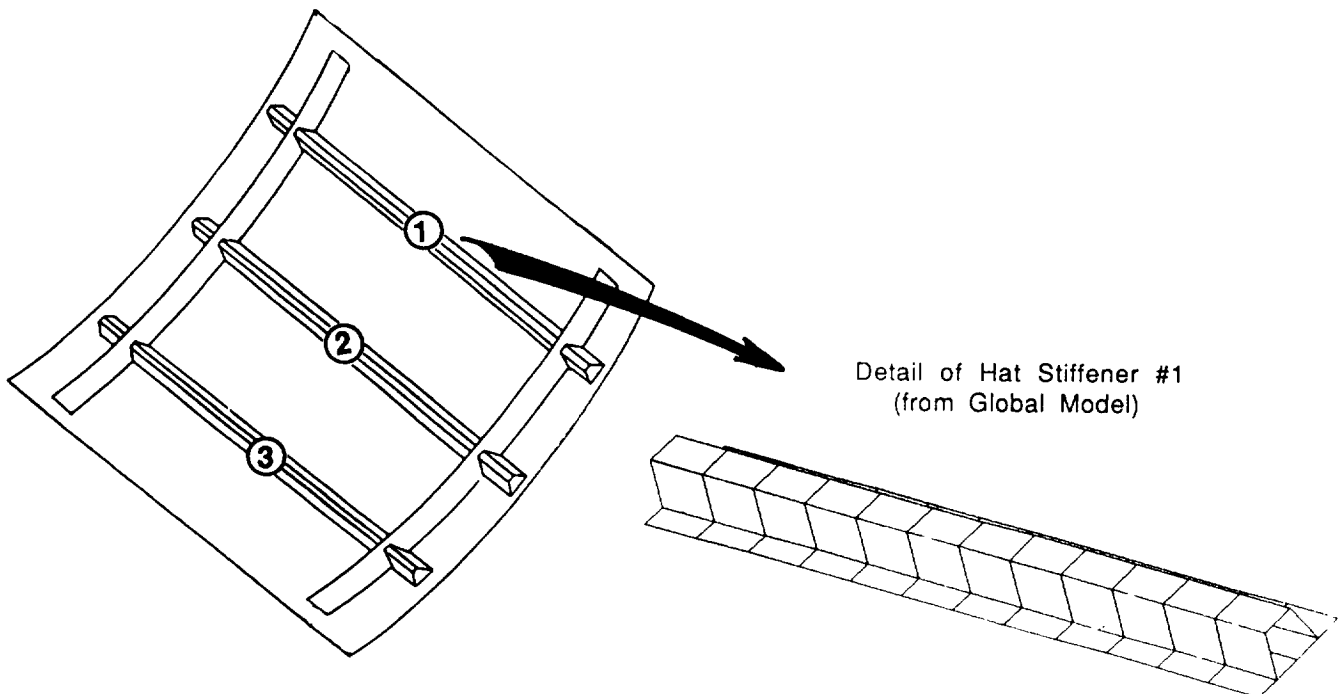


Figure 9

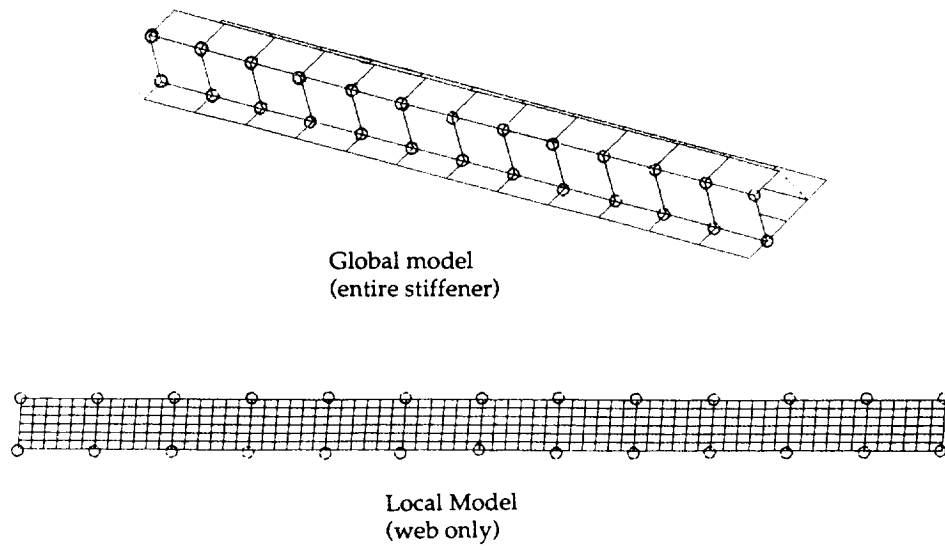


Figure 10

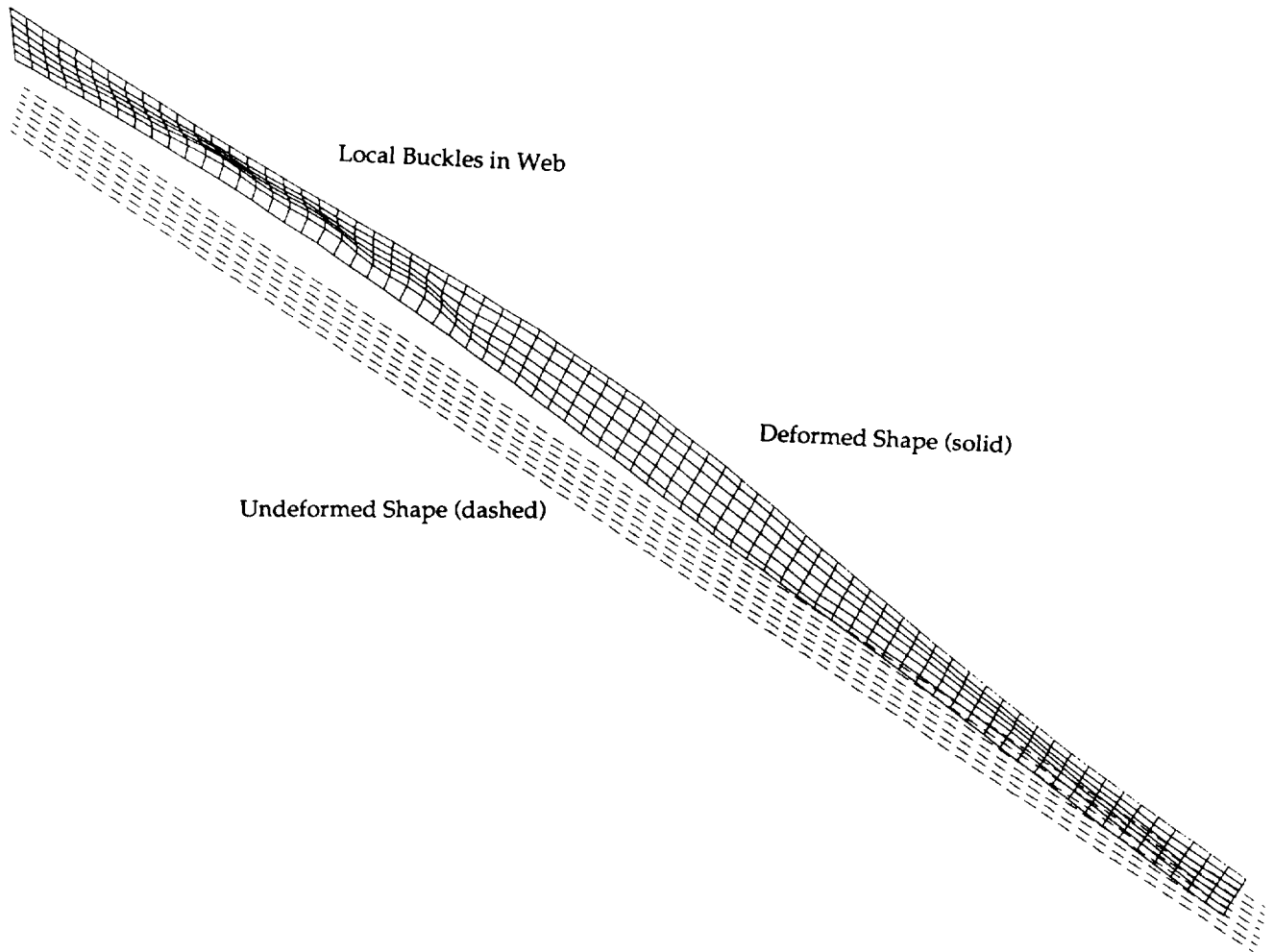
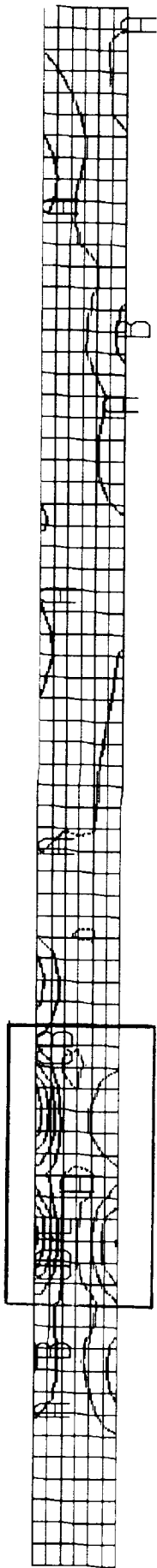
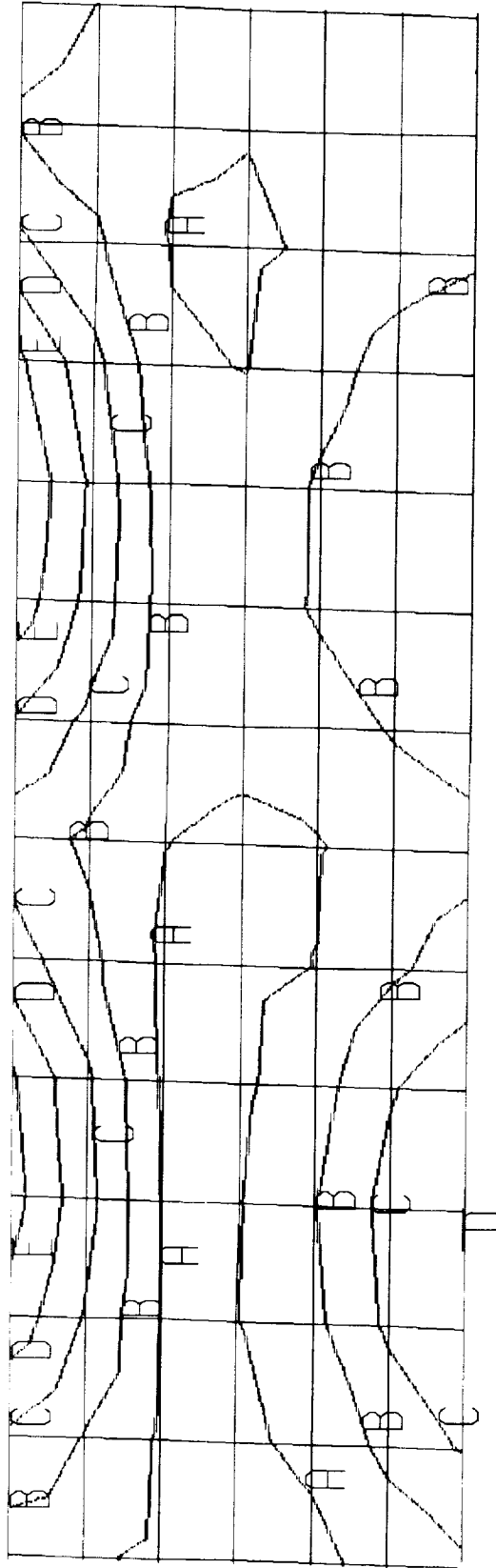


Figure 11



Overall



Detail

Contour Letter	Hoffman Failure Number (Mean)
A	0.750
B	0.583
C	0.416
D	0.250
E	0.082

FIGURE 12

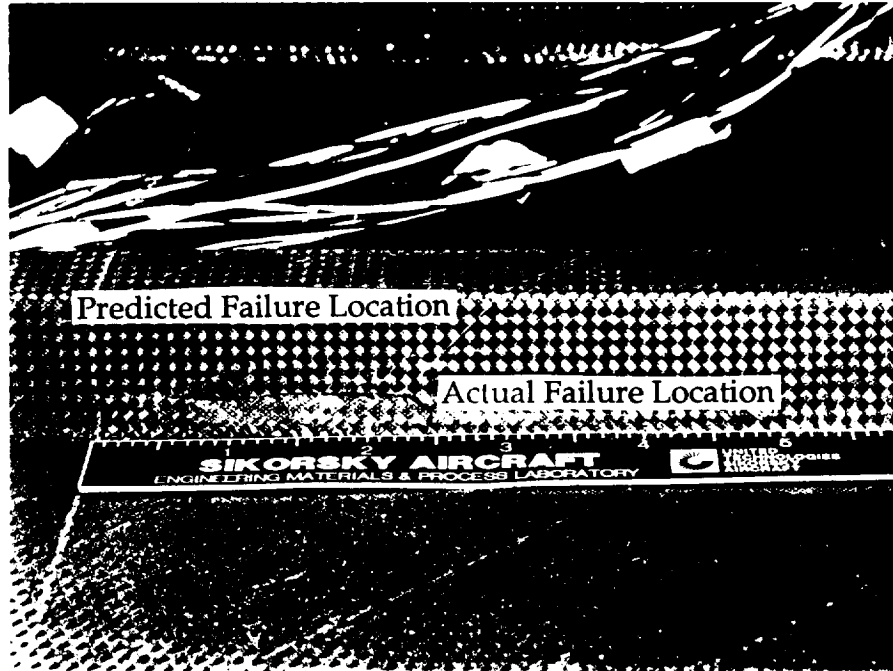


FIGURE 13

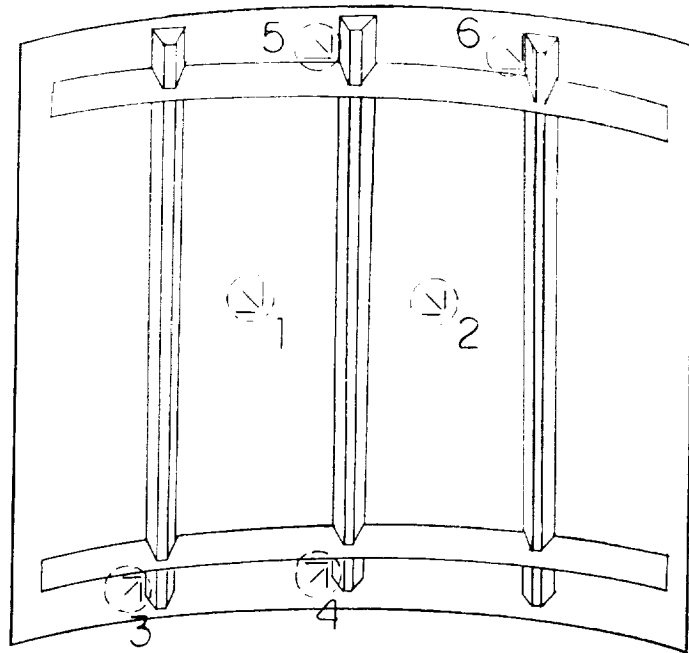


Figure 14

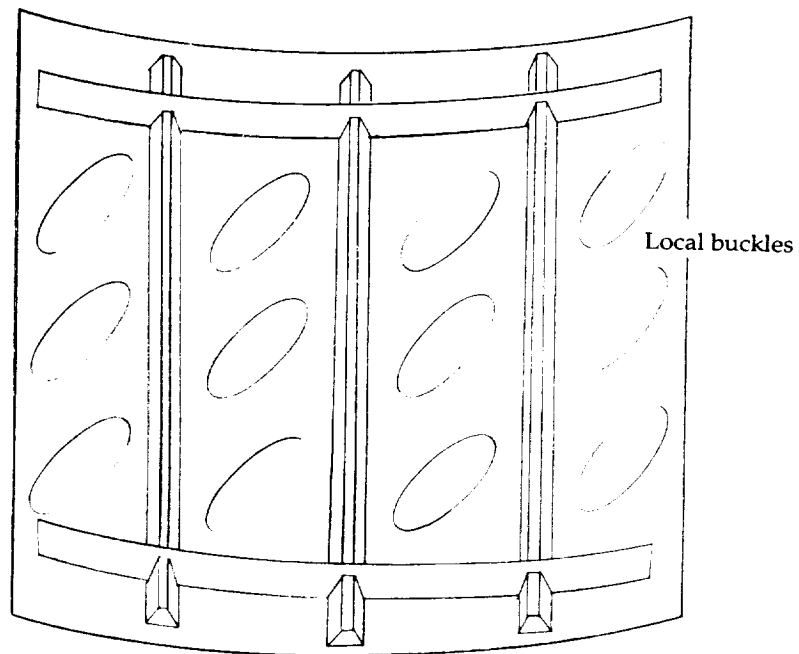


Figure 15

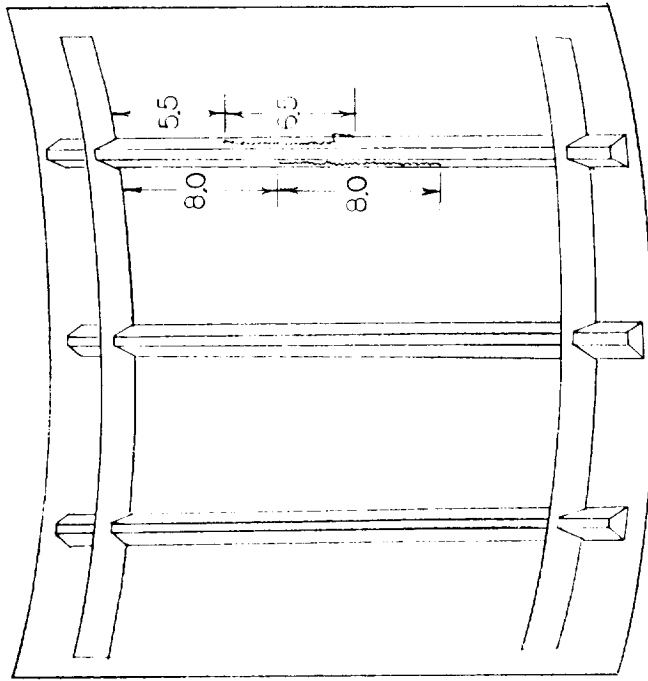


Figure 17

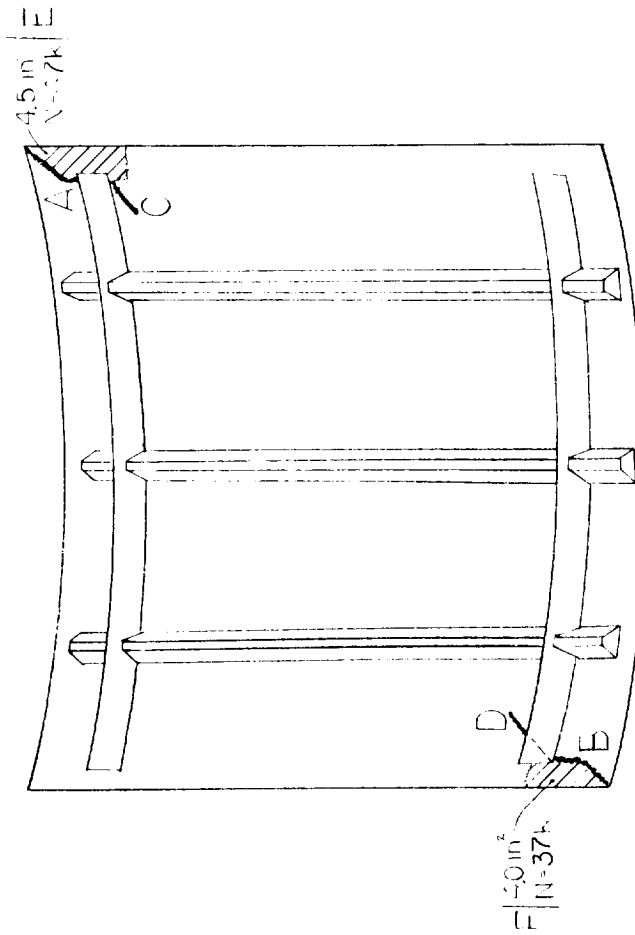


Figure 16

Crack	Crack Length [in]			
	1 cycle	10 cycles	100 cycles	1,000 cycles
A	1.50	1.50	2.75	2.75
B	1.50	1.50	0.75	0.50
C	-----	-----	0.50	0.50
D	-----	-----	0.50	0.50

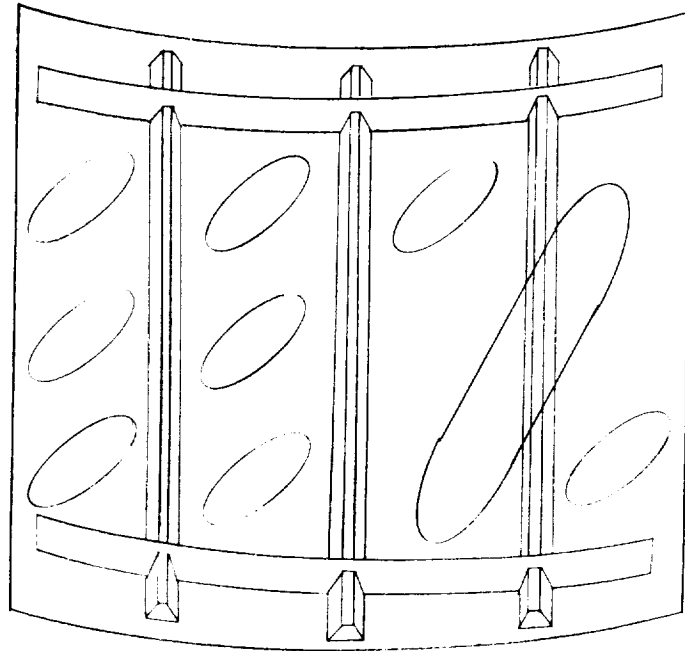


Figure 18

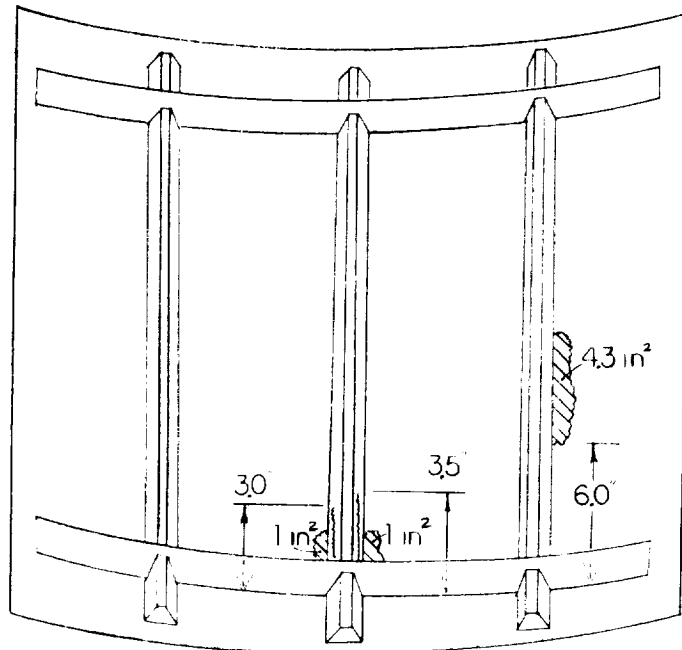


Figure 19

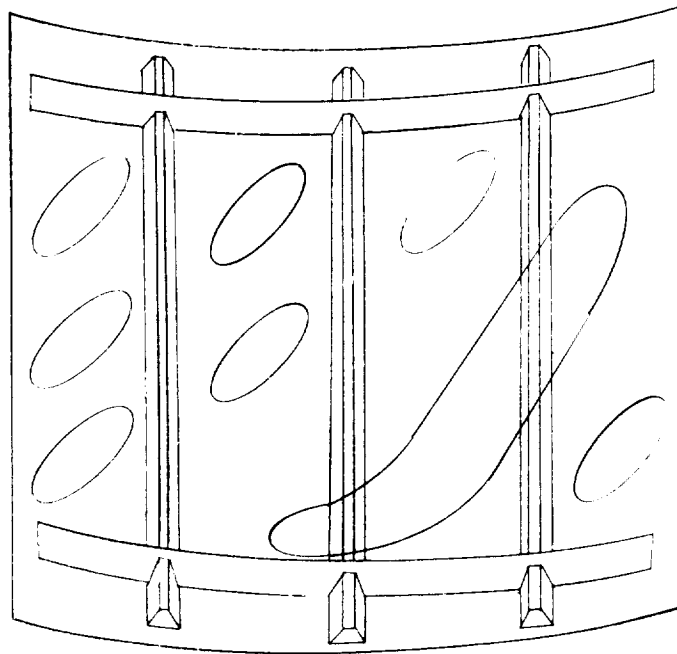


Figure 20

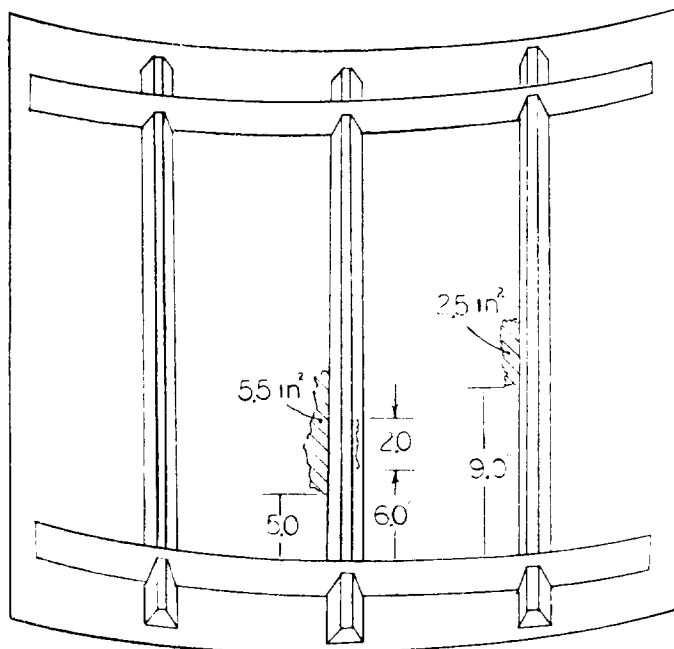
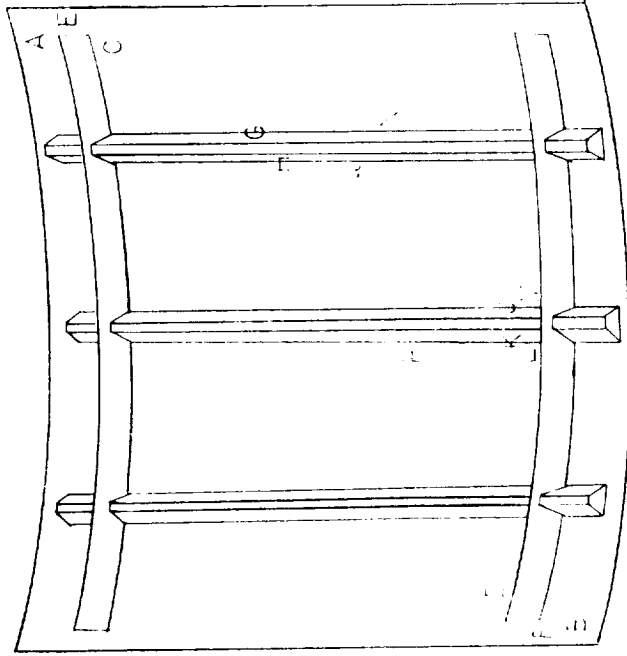
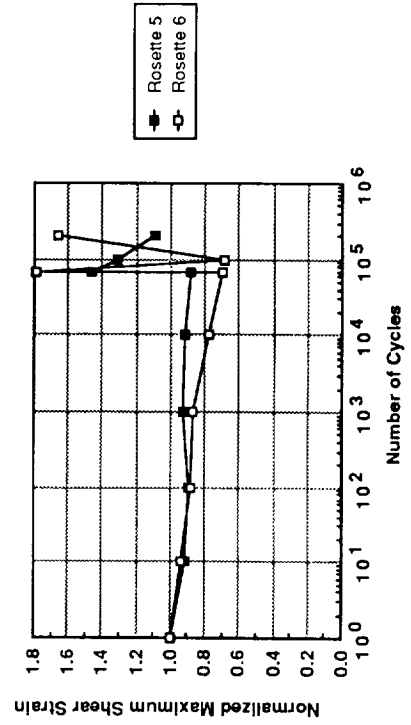
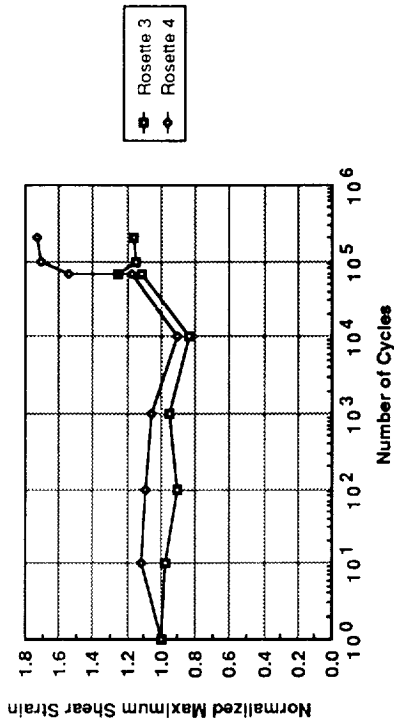
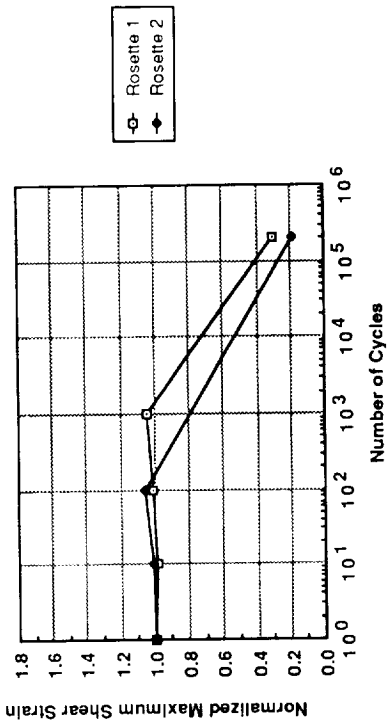


Figure 21



Damage Site	Type	Final Size
A	Crack	2.8 in
B	Crack	2.5 in
C	Crack	2.0 in
D	Crack	2.5 in
E	Delam	4.5 in**2
F	Delam	4.0 in**2
G	Crack	6.5 in
H	Crack	8.0 in
J	Crack	5.5 in
K	Crack	3.0 in
L	Delam	1.0 in**2
M	Delam	1.0 in**2
N	Delam	4.3 in**2
P	Delam	5.5 in**2
Q	Delam	2.5 in**2

Figure 23

Figure 22